

Original Article

Preparation and pharmacokinetics *in vivo* of linarin solid dispersion and liposomeYingying Huang^{a,1}, Lihua Xu^{a,1}, Fangping Zhang^a, Yang Liu^{a,b}, Yunyu Wang^a, Fangfeng Meng^a, Shuang Li^a, Xintao Cheng^a, Yuefeng Bi^{a,b,*}^aSchool of Pharmaceutical Sciences, Zhengzhou University, Zhengzhou 450001, China^bCollaborative Innovation Center of New Drug Research and Safety Evaluation, Zhengzhou 450001, China

ARTICLE INFO

Article history:

Received 7 April 2021

Revised 16 August 2021

Accepted 28 December 2021

Available online 2 April 2022

Keywords:

bioavailability

intestinal absorption

linarin

liposome

pharmacokinetics

solid dispersion

ABSTRACT

Objective: The current investigation aimed to determine the appropriate dosage form by comparing solid dispersion and liposome to achieve the purpose of improving the solubility and bioavailability of linarin. **Methods:** Linarin solid dispersion (LSD) and linarin liposome (LL) were developed via the solvent method and the thin film hydration method respectively. The Transwell chamber model of Caco-2 cells was established to evaluate the absorption of drug. The pharmacokinetics of linarin, LSD and LL in rats after ig administration were carried out by high performance liquid chromatography (HPLC) method.

Results: The solubility of LSD and LL was severally 3.29 times and 3.09 times than that of linarin. The permeation coefficients of LSD and LL were greater than 10^{-6} , indicating that the absorption of LSD and LL were both better than linarin. The bioavailability of the LSD was 3.363 times higher than that of linarin, and the bioavailability of LL was 0.9886 times higher than that of linarin.

Conclusion: The linarin was more suitable for making solid dispersion to enhance its solubility and bioavailability.

© 2022 Tianjin Press of Chinese Herbal Medicines. Published by ELSEVIER B.V. This is an open access article under the CC BY-NC-ND license (<http://creativecommons.org/licenses/by-nc-nd/4.0/>).

1. Introduction

Flavonoids are an important type of natural organic compounds and exist widely in nature (Shao, Ting, Wang, Sun, & Guo, 2020; Zanoaga et al., 2019; Yi, 2018). Even if studies show that flavonoids have extensive pharmacological actions, such as anti-oxidation (Chanput, Krueyos, & Ritthiruangdej, 2016), anti-tumor (Wang et al., 2017), anti-aging (Tang, Wang, Gao, Wang, & Zhao, 2017), its application is still restricted as a result of molecular structure and existence status which brings about solubility difficulties (Tian et al., 2019; Uifálean et al., 2016; Li et al., 2017; Guo, Zhang, Guan, & Zhou, 2019; S, F, Z, Z & Z, 2018). Linarin (7-[[6-O-(6-deoxy- α -L-mannopyranosyl)- β -D-glucopyranosyl]oxy]-5-hydroxy-4'-methoxyflavone) (Fig. 1), which is one of the main active ingredients and index ingredients in *Chrysanthemi Indici Flos*. It has a wide range of physiological and pharmacological activities, such as preventing diabetes, protecting the liver, inhibiting phosphodiesterase and aldose reductase and resisting bacteria, etc (Zhen et al., 2017; Wang et al., 2018; Xie, Yang, Wei, Xu, & Qin,

2020; Feng et al., 2018;). It also has a certain effect on chronic bronchitis and hyperlipidemic (Das das Graças C de Souza, Cyrino, de Carvalho, Blanc-Guillemaud, & Bouskela, 2018; Li, Guang, Zhao, Feng, & Qiu, 2019). Our early laboratory research also has shown that linarin had remarkable hypoglycemic activity. Despite exerting a range of therapeutic effects, linarin possesses restricted commercial viability owing to its low oral bioavailability caused by poor water solubility. This is due to its special structure, a flavonoids with two sugars at C-7 position, which results both in poor lipid and water solubility and extremely low bioavailability. Therefore, seeking appropriate dosage forms to overcome this limitation has become a pressing challenge in clinical application of linarin.

The concept of solid dispersion first appeared in 1961. The preparation of solid dispersions is the simplest and most effective way to improve solubility, dissolution rate and bioavailability of drugs. The main advantages are that the reduction of particle size can reduce the transformation of the drug from crystalline to amorphous state and enhance the wettability and porosity (Rumondor, Marsac, Stanford, & Taylor, 2009; Vasconcelos, Sarmiento & Costa, 2007; Onoue et al., 2010; Indulkar, Lou, Zhang & Taylor, 2019; Choi, Lee, Jang, Byeon, & Park, 2018; Mesallati, Umerska, Paluch, & Tajber, 2017). Study has prepared the solid

* Corresponding author.

E-mail address: zzubyf@126.com (Y.f. Bi).¹ These authors contributed equally to this work.

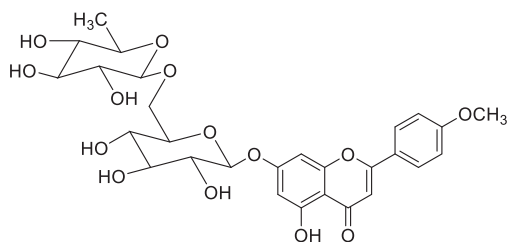


Fig. 1. Chemical structure of linarin.

dispersions by melting method with the mass ratio of linarin and polyethylene glycol (peg) 6000 as 1:9. The results showed that the linarin solid dispersions prepared by peg 6000 as the carrier can significantly improve the dissolution rate of linarin *in vitro*, and they were evenly distributed in the carrier with supersaturation solid solution or amorphous state (Wang, Jun, Zhang, & Amp, 2013). On the contrary novel targeted drug delivery system such as liposome can achieve the goals of improving drug safety, effectiveness, stability, patient compliance, and reducing adverse drug reactions (Sun & Jin, 2009; Vergara & Shene, 2019; Tai et al., 2019). Due to numerous advantages, liposome had received an increasingly attention from the medical community domestic and foreign (Li et al., 2019; Zeng et al., 2017). Hence solid dispersion and liposome were selected as the formulation research of linarin in this experiment.

In briefly, we developed linarin solid dispersion and liposome successfully. The solid dispersion and liposome were characterized using various techniques, and the solubility, drug absorption, and bioavailability were compared to determine linarin dosage form with enhanced solubility and bioavailability.

2. Materials and methods

2.1. Chemicals and reagents

Linarin was isolated and purified by our laboratory. The structure was identified by ^1H NMR (Fig. S1) and ^{13}C NMR (Fig. S2). The content was more than 98% by HPLC (Fig. S3); PVP_{K30} (Shanghai Lanji Technology Development Co., Ltd., Shanghai, China); Polosham (Anhui Shanhe Accessories, Anhui, China); Methanol (Tianjin Damao Chemical Reagent Factory, Tianjin, China); Acetonitrile (Tianjin Komio Chemical Reagent Co., Ltd., Tianjin, China); Dimethyl sulfoxide (DMSO) (Chromatographic grade, Tianjin Komio Chemical Reagent Co., Ltd., Tianjin, China); Phosphoric acid (analytical grade, Tianjin Komio Chemical Reagent Co., Ltd., Tianjin, China); Soy Lecithin (Shanghai Taiwei Pharmaceutical Co., Ltd., Shanghai, China); Cholesterol (Sinopharm Chemical Reagent Co., Ltd., Shanghai, China); Dulbecco's modified eagle medium (DMEM) medium (ThermoFly); Fetal bovine serum (Beijing Wobisen Technology Co., Ltd., Beijing, China); Trypsin (Shandong Sukehan Bioengineering Co., Ltd., Shandong, China); Hanks buffer (Shanghai Xinyu Biotechnology Co., Ltd., Shanghai, China); All other reagents were of analytical grade and used as received.

2.2. Cells

The Caco-2 cell line was provided by PhD Xiaotian Li, School of Pharmacy, Zhengzhou University, China. It was cultured in 5% CO_2 , 37 °C constant temperature incubator.

2.3. Animals

SPF-grade 6–8 week old KM male rats (0.2 ± 0.02) kg (Animal quality certificate number: 41003100003179), provided by Henan

Experimental Animal Center [Animal production license number: SCXK (Yu) 2017-0001]. The research protocol was reviewed and approved by the Ethics Committee of Zhengzhou University. Feeding conditions: Animal feeding room of individually ventilate cages (IVC) system of Zhengzhou University Pharmaceutical Research Institute [Experimental animal use license number: SYXK (Yu) 2018-0004], IVC was housed in an independent air-separated cage and can drink water and eat freely. The room temperature in the animal room was (20–25) °C, the relative humidity was 40%–70%, the light was natural light, 12 h light/12 h dark.

2.4. Preparation of LSD

Linarin and PVP_{K30} were weighed and mixed uniformly in a mortar according to the ratio of the drug to the carrier (1:3) and dissolved in an appropriate amount of 70% ethanol. The solvent was evaporated and dried for 10 h. The linarin solid dispersion (LSD) was pulverized, passed through a 200 mesh sieve, and was placed in a vacuum desiccator.

2.5. Characterization of LSD

2.5.1. DSC analysis

The thermal study was conducted using a DSC-60A Differential Scanning Calorimeter (Shimadzu Enterprise Management Co., Ltd., Shanghai, China) at a heating rate of 10 °C/min. Aluminum bismuth was the reference cell; Al_2O_3 was the reference material; Scanning environment, N_2 atmosphere, 30–300 °C.

2.5.2. FTIR analysis

The IR fingerprint of linarin, PVP_{K30}, physical mixture and LSD were obtained using an Thermo Scientific Nicolet iS10 Fourier Transform Infrared Spectroscopy with KBr as a reference. The wavelength range was 400 cm^{-1} – 4000 cm^{-1} .

2.5.3. TEM analysis

Sample's morphology was taken using Transmission Electron Microscope, 1200EX (Japan).

2.5.4. PXRD analysis

X-ray data were generated using Bruker D8 ADVANCE (Bruker, Germany). The 2 θ range was over the 5–90 and at a scan speed of 4 deg/min. Cu with $K\alpha = 1.5406$ nm monochromatized as graphite crystal for the tube anode. The peak patterns were collected for each sample under the following conditions: the voltage of 40 kV, tube current of 40 mA, step size of 0.02, counting time of 0.3 s/step.

2.5.5. In vitro drug dissolution

Linarin, LSD and physical mixture were weighted and placed in a cup containing 900 mL of distilled water, maintain at (37 ± 0.5) °C. The sample (5 mL) was received and filtered through 0.22 μm at 2, 7, 12, 27, 42 and 60 min respectively. RC-6 drug dissolution tester (Tianjin Optical Instrument Factory, Tianjin, China) was used to test *in vitro* drug dissolution. The concentrations of drug were tested by HPLC (Waters-2695 USA HPLC system). A column of YMC C₁₈ column (250 mm \times 4.6 mm, 5 μm) was used with column temperature: 25 °C; mobile phase: 0.5%; phosphate buffer-acetonitrile (70:30, volume percentage); flow rate: 1.0 mL/min; detection wavelength: 340 nm; injection volume 10 μL .

2.6. Preparation of LL

The prescribed amount of linarin and excipients were weighed and 10 mL methanol was added. The solvent was evaporated by heating at 40 °C. Later, 4 mL PBS (pH 7.2) solution was added

and hydrated for 1 h at the suitable temperature to obtain linarin liposome (LL) dispersions. The prepared LL dispersion was probed in an ice bath.

2.7. Evaluation of LL

2.7.1. TEM analysis

Sample's morphology was taken using TEM, 1200EX (Japan).

2.7.2. Measurement of particle size distribution and potential

The particle size and potential distribution of the sample were obtained by laser nanoparticle size analyzer. LL was taken and diluted with distilled water. The laser particle size analyzer was used to measure the average particle size and distribution which was required to be less than 200 nm.

The Zeta potential was required to be a negative value. The larger the absolute value of the Zeta potential is, the more mutually repelling the liposome particles are, the more stable the liposome system is, and the less prone to aggregation is.

2.8. Solubility of linarin, LSD and LL

Linarin, LSD and LL were placed in 10 mL of conical flask respectively ($n = 6$), 5 mL distilled water was added in each flask, shaking at 100 r/min, 37 °C for 24 h. At the time point of 0.5, 1.5, 2.5, 4.5, 8.5, 12.5 and 24.5 h, the supernatant was obtained and filtered through a 0.22 μm microporous membrane, and the solubility of linarin, LSD and LL were measured by HPLC method.

2.9. Caco-2 cell transport experiment of linarin, LSD and LL

The 21-day-differentiated Caco-2 monolayer was used to measure the resistance value, and the drug absorption and transport experiments were performed.

AP side \rightarrow BL side: linarin, LSD and LL HBSS solution (100 μm) were added to the supplying side (AP side: 0.5 mL) and the receiving side (BL side: 1.5 mL). The blank HBSS solution of BL side was used as the receiving liquid. At 0, 15, 30, 45, 60, 90 and 120 min, 1.2 mL sample were taken at the receiving end while an equal volume of HBSS solution was replenished. Three wells were paralleled at each time point and the supernatant was taken to test the drug concentration by HPLC (Waters-2695 USA HPLC system). A column of YMC C₁₈ column (250 mm \times 4.6 mm, 5 μm) was used with column temperature: 25 °C; mobile phase: 0.5%; phosphate buffer-acetonitrile (70:30, volume percentage); flow rate: 1.0 mL/min; detection wavelength: 340 nm; injection volume 10 μL .

BL side \rightarrow AP side: linarin, LSD and LL HBSS solution were added to the supplying side (BL side: 1.5 mL), and the blank HBSS solution was added to the receiving side (AP side: 0.5 mL). At 0, 15, 30, 45, 60, 90 and 120 min, 0.4 mL sample were taken on the receiving end while an equal volume of HBSS solution was replenished. The supernatant was taken to test the drug concentration by HPLC (Waters-2695 USA HPLC system). A column of YMC C₁₈ column (250 mm \times 4.6 mm, 5 μm) was used with column temperature: 25 °C; mobile phase: 0.5%; phosphate buffer-acetonitrile (70:30, volume percentage); flow rate: 1.0 mL/min; detection wavelength: 340 nm; injection volume 10 μL .

Data processing:

Calculation of P_{app} (cm/s):

$$P_{\text{app}} = \frac{dQ/dt}{A \times \rho_0} \quad (1)$$

Where dQ/dt is the rate of appearance of the drug in the sink, A is transmembrane cross-sectional area and ρ_0 is initial concentration

at the supply side. Among them, P_{app} (BL-AP) and P_{app} (AP-BL) were the apparent permeability coefficients of drug transport from BL side to AP side and AP side to BL side, respectively. The above results were expressed by mean \pm SD. Differences in data between groups One-way analysis of variance. The permeability was increased with the P_{app} value. The test was used to compare the two sets of data, and the results were expressed as mean \pm SD. Drugs with an apparent permeability coefficient greater than (1×10^{-6}) cm/s indicate good absorption.

2.10. Pharmacokinetic study of linarin, LSD and LL in vivo

Male Wister rats were randomly divided into three groups, six in each group, and fasted for 12 h before experiment, free drinking water. linarin, LSD and LL (equivalent to 50 mg/kg linarin) were ig administrated to the rats. 0.7 mL blood sample was drawn through the retro-orbital plexus vein at time intervals of 0.5, 1, 1.5, 2, 4, 6, 8, 12 and 24 h after administration, centrifuged (4000 r/min, 10 min), collected the plasma and stored at -20 °C.

2.10.1. Plasma sample treatment

Methanol (1.5 mL) was added to 200 μL plasma to precipitate protein, vortexed and mixed for 3 min, centrifugated for 10 min (10 000 r/min). The supernatant was blow-dried by nitrogen at room temperature. The residue was redissolved in 200 μL methanol, vortexed for 2 min, and centrifuged for 10 min (12 000 r/min). The supernatant was detected by HPLC.

2.10.2. Chromatography conditions

The linarin in plasma was detected by HPLC. Chromatographic separation was performed on (Agilent) C₁₈ column (250 mm \times 4.6 mm, 5 μm). The mobile phase consisted of acetonitrile and 0.5% phosphate buffer (40/60, v/v, pH = 5.00) with a flow rate of 1.0 mL/min and column temperature of 30 °C. The injection volume was 10 μL and detection wavelength was 340 nm.

2.10.3. Time-course curve and pharmacokinetic parameters

After the oral administration of linarin, LSD and LL, the pharmacokinetic parameters and relative bioavailability were calculated by PKSolver software ($n = 6$).

3. Results and discussion

3.1. Characterization of LSD

3.1.1. DSC, FTIR, TEM PXRD analysis

The distribution of drug crystals in LSD was detected by differential scanning calorimetry (DSC) (Fig. 2). linarin had an endothermic peak near 259 °C, which was the characteristic peak of linarin melting point. Polyvinylpyrrolidone K30 (PVP_{K30}) had an obvious endothermic peak at 56 °C. There was no characteristic absorption peak of linarin in the physical mixture, but an absorption peak at about 103 °C. It was preliminarily speculated that there was a low eutectic between the API and the components in the physical mixture. In LSD, there was no characteristic peak of linarin melting point and eutectic peak, indicating that the substance and the carrier formed a new phase. Linarin existed in the carrier in an amorphous form, suggesting that the special network skeleton structure of PVP series substances inhibited drug crystallization.

At the same time, FTIR detected possible molecular interactions within LSD (Fig. 2). The relevant absorption peaks of linarin in the infrared spectrum were: 3470 cm^{-1} stretching vibration of phenol hydroxyl group, 2936 cm^{-1} stretching vibration of saturated C-H bond, 1659 cm^{-1} C=O stretching vibration, and 1500 cm^{-1} – 1607 cm^{-1} stretching vibration of benzene ring. The asymmetric

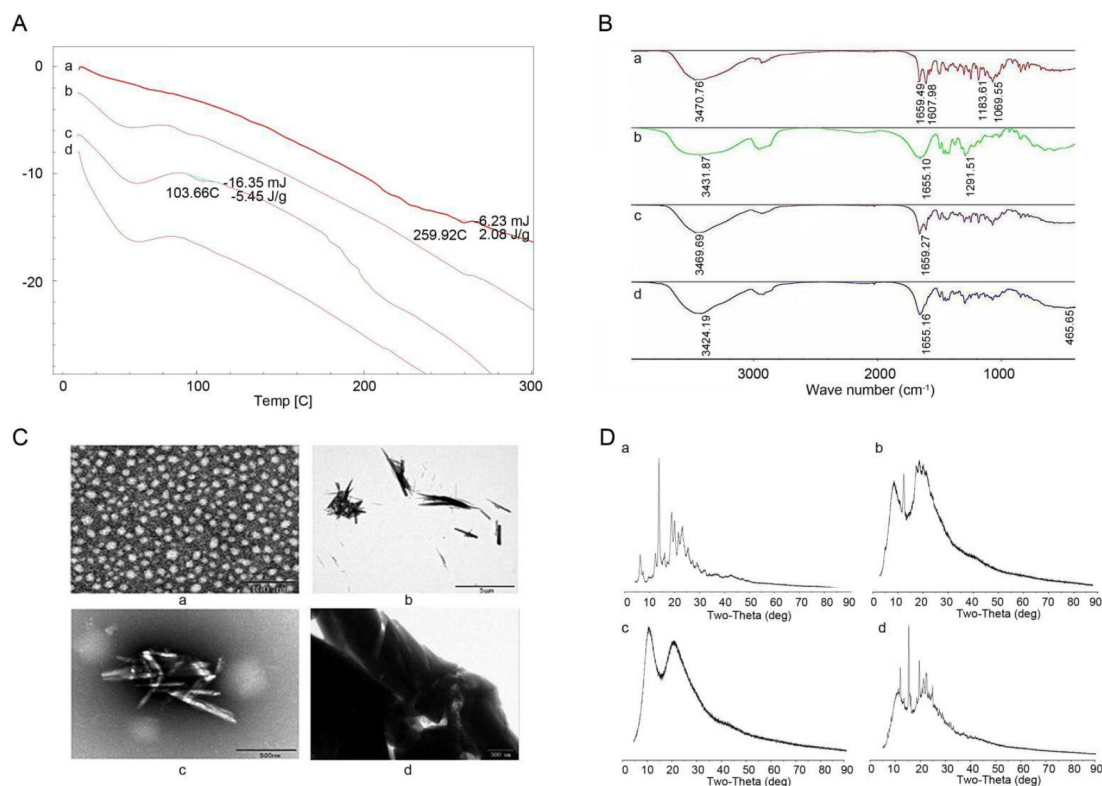


Fig. 2. A: DSC diagram of linarin (a), PVP_{K30} (b), physical mixture (c) and LSD (d); B: FTIR map of linarin (a), PVP_{K30} (b), physical mixture (c) and LSD(d); C: Transmission electron micrograph of PVP_{K30} (a), linarin (b), physical mixture (c) and LSD (d); D: X-ray diffractograms (PXRD) of linarin (a), PVP_{K30} (b), physical mixture (c) and LSD (d).

deformation vibration of CH₃ was 1470 cm⁻¹–1440 cm⁻¹, and 1150 cm⁻¹ was the stretching vibration of aliphatic tertiary alcohols. From 1037 cm⁻¹ to 1069 cm⁻¹ were the asymmetric stretching vibrations of aromatic ether. In the infrared spectrum of PVP_{K30}, there was an absorption peak generated by OH stretching vibration at 3431 cm⁻¹, and a C=O stretching vibration peak at 1655 cm⁻¹. Although these peaks still exist in the physical mixture and their position and strength did not change significantly, it indicated that the API was simply mixed with PVP_{K30}. In LSD, the phenol hydroxyl peak widened slightly, and the C=O characteristic peak weakened. It was preliminarily inferred that the hydrogen bond effect occurred in the interior of the material, resulting in the weakening of the characteristic peak and the shift to the low wave number direction. Furthermore, as a result of this association, energy is released and the drug is present in an amorphous form in the carrier.

According to TEM analysis results (Fig. 2), the physical mixture is only a simple mixture of linarin and PVP_{K30}. However, the state of substances in LSD was different from that of physical mixtures.

Due to the change of the association mode between substances, linarin was dispersed in the form of microcrystals in the carrier.

In order to investigate crystalline state, p-XRD studies were carried out (Fig. 2). The crystal peaks of the drug were still visible in the LSD, demonstrating that the drug was dispersed in the form of microcrystals in the solid dispersion. The result was consistent with that obtained by TEM.

Therefore, phenotypic results indicated that in LSD, a new phase was formed between the linarin and the carrier and existed in the form of microcrystals in the carrier.

3.1.2. In vitro drug dissolution

RC-6 drug dissolution detector was used to test *in vitro* drug dissolution (Fig. 3). At 10 min, the cumulative dissolution of the LSD reached 75.06%, however, the cumulative dissolution of the physical mixture and the linarin was 66.66% and 62.50%, respectively. The result showed that the dissolution rate of the LSD, compared to linarin and physical mixture, was significantly improved.

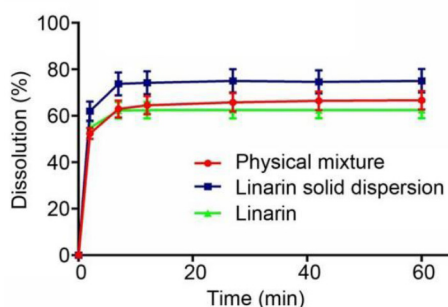


Fig. 3. Dissolution of linarin, LSD and physical mixture.

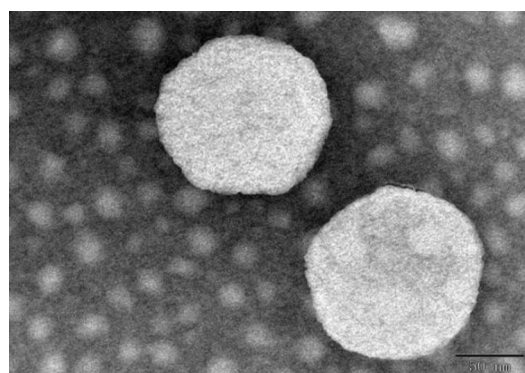


Fig. 4. Transmission electron micrograph of LL.

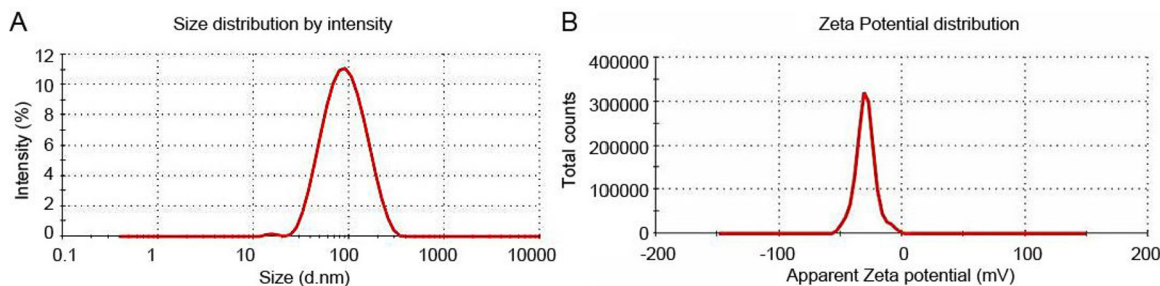


Fig. 5. Particle size (A) and electric potential (B) distribution of LL.

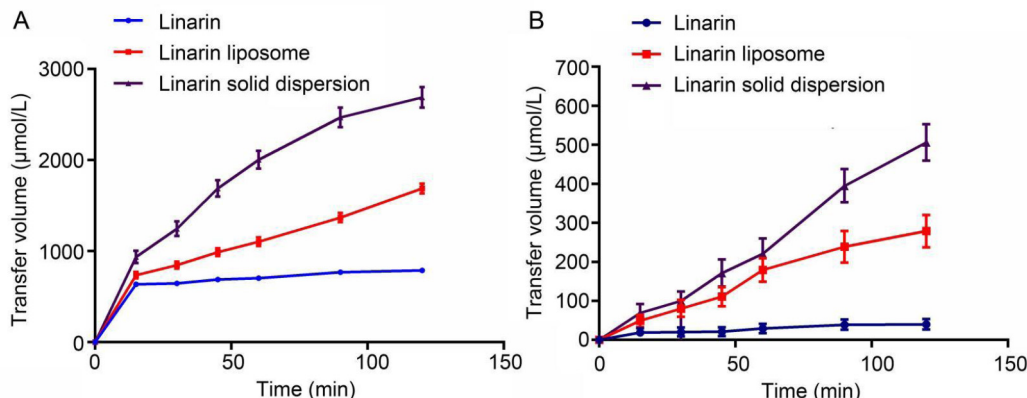


Fig. 6. Caco-2 cell transport experiment of linarin, LSD and LL. AP-BL side transshipment of LSD-LL-linarin (A); BL-AP side transshipment of LSD-LL-linarin (B).

Table 1
Water solubility of linarin, LSD and LL.

Dosage forms (µg/mL)	Formulations			Mean ± SD
	1	2	3	
Crude drug	0.0590	0.0603	0.0590	0.0594 ± 0.0007
Solid dispersion	0.1960	0.1940	0.1974	0.1958 ± 0.0017
Liposome	0.1860	0.1840	0.1830	0.1843 ± 0.0012

3.2. Evaluation of LL

3.2.1. TEM

LL was distributed in a spherical shape with uniform particle size and less adhesion (Fig. 4).

3.2.2. Measurement of particle size distribution and potential

The particle size of the LL was 80.33 nm and the electric potential was -29.4 mV, manifesting that the LL was evenly distributed and had good stability (Fig. 5).

3.3. Solubility of linarin, LSD and LL

Solvent method and thin film hydration method were used to prepare LSD and LL, respectively. It can be seen from Table 1 that the solubility of LSD was 0.1958 µg/mL, which was 3.29 times that of linarin (0.0595 µg/mL). The solubility of LL was 0.1840 µg/mL, which was 3.09 times that of linarin (0.0595 µg/mL). The solubility data showed that the solubility of the poorly soluble drug can be significantly improved after combining the poorly soluble drug with the carrier.

3.4. Caco-2 cell transport experiment of linarin, LSD and LL

The Transwell chamber model of Caco-2 cells was established to evaluate the absorption of drug. The absorption of linarin, LSD and

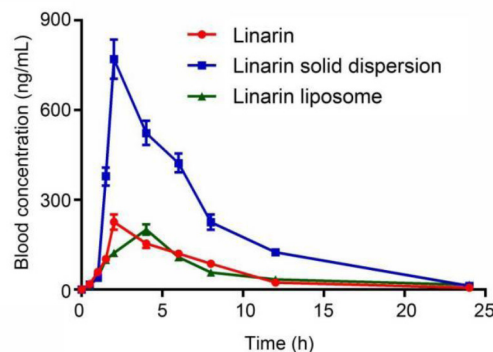


Fig. 7. Plasma drug concentration–time curve of linarin, LSD and LL after ig administration in rats (mean ± SD, n = 6).

LL *in vitro* were presented in Fig. 6. At 120 min, the average apparent permeability coefficient (P_{app}) of linarin, LSD and LL from AP side to BL side was 8.499×10^{-10} , 5.928×10^{-5} and 6.070×10^{-3} , respectively. The mean P_{app} values of linarin, LSD and LL from BL side to AP side were 2.960×10^{-11} , 3.120×10^{-7} and 1.57×10^{-7} , respectively. The permeability coefficient of LSD from AP side to BL side was 6.975×10^5 times that of linarin. The permeability coefficient of LL from AP side to BL side was 7.142×10^6 times that of linarin. The permeability coefficients of LSD and LL were both greater than 10^{-6} , indicating that the absorption of LSD and LL was good. The carrier encapsulated insoluble drugs could significantly promote the absorption of insoluble drugs.

3.5. Pharmacokinetic study of linarin, LSD and LL *in vivo*

Fig. 7 showed the plasma drug concentration–time curve of linarin, LSD and LL in rats. The pharmacokinetics of linarin, LSD

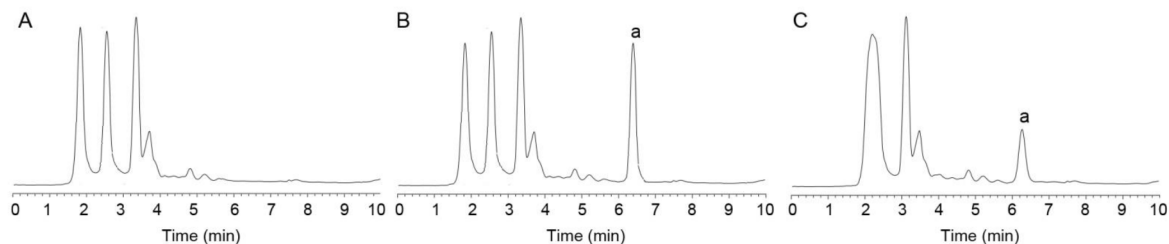


Fig. 8. Method specificity (A: blank plasma; B: blank plasma with linarin; C: 2 h plasma sample of rat; a: linarin).

Table 2

Pharmacokinetic parameters of linarin, LSD and LL.

Parameters	Linarin	Linarin solid dispersion	Linarin liposome
C_{max} (ng/mL)	226.2	970.6	200.7
T_{max} (h)	2.000	2.000	4.000
$t_{1/2}$ (h)	4.117	4.211	9.200
$AUC_{(0-24)}$ (ng·h/mL)	1407	4733	1391
$MRT_{(0-24)}$ (h)	6.707	5.997	11.39
CL (mL/h)	0.5717	0.1716	0.5140

and LL after intragastric administration in rats were determined by high performance liquid chromatography (Fig. 8). The pharmacokinetic parameters were shown in Table 2. The results showed that the bioavailability of LSD was 3.363 times that of linarin, and the bioavailability of LL was 0.9886 times that of linarin. The AUC, C_{max} and CL of LL were lower than that of linarin. It indicated that the release rate was relatively slow, and it took a long time to reach the main absorption site of the drug, which further showed that it will have a sustained release effect. However, the increase of C_{max} and AUC of LSD indicated that the release rate was greater than the absorption rate, which made the plasma concentration and bioavailability increase rapidly. The release rate of the drug in the LL was less than the rate of absorption, so the blood concentration of LL was lower, the longer the half-life of the plasma concentration was, the longer the drug molecules stayed in the body, and the bioavailability was lower. For flavonoids, which are difficult to absorb drugs, it is not suitable to be made into liposomes with sustained release effect, which will reduce the bioavailability. It is more suitable to add water-soluble carriers to increase its solubility and bioavailability.

4. Conclusion

In the present study, we successfully developed LSD and LL by solvent method and thin-film dispersion method separately. The formulations were also characterized using various characterization techniques, including DSC, p-XRD, FTIR, DLS and TEM. Vitro solubility and Caco-2 cells transport experiment results demonstrated that the solubility and absorption of LSD and LL were significantly improved, while the pharmacokinetic experiment indicated that LSD displayed much higher oral bioavailability, which was superior compared with LL. The sustained release effect of LL probably resulted in this outcome. Through the comparison of vitro solubility, intestinal absorption, and pharmacokinetic experiments *in vivo* determined an appropriate dosage form (LSD) which suit linarin to improve the solubility and bioavailability. In summary, this research provided some scientific basis for the research of other preparations of linarin and offered some ideas for the research of similar insoluble flavonoids simultaneously.

Author contributions

All authors have read and agreed to the published version of the manuscript.

Declaration of Competing Interest

The authors declare that they have no known competing financial interests or personal relationships that could have appeared to influence the work reported in this paper.

Acknowledgements

The Authors are very grateful to the technical support received from professor Lei Fu, School of Pharmaceutical Sciences, Zhengzhou University, China.

This study was financed by Natural Science Foundation of Henan Province (Grant No. 182300410348).

Appendix A. Supplementary data

Supplementary data to this article can be found online at <https://doi.org/10.1016/j.chmed.2021.12.004>.

References

- Chanput, W., Krueyos, N., & Ritthiruandej, P. (2016). Anti-oxidative assays as markers for anti-inflammatory activity of flavonoids. *International Immunopharmacology*, 40, 170–175.
- Choi, J. S., Lee, S. E., Jang, W. S., Byeon, J. C., & Park, J. S. (2018). Solid dispersion of dutasteride using the solvent evaporation method: Approaches to improve dissolution rate and oral bioavailability in rats. *Materials Science & Engineering C, Materials for Biological Applications*, 90, 387–396.
- Das das Graças C de Souza, M., Cyrino, F. Z., de Carvalho, J. J., Blanc-Guillemard, V., & Bouskela, E. (2018). Protective effects of micronized purified flavonoid fraction (MPFF) on a novel experimental model of chronic venous hypertension. *European Journal of Vascular and Endovascular Surgery*, 55(5), 694–702.
- Feng, X. C., Li, Y., Guang, C. X., Qiao, M., Wang, T., Chai, L. W., & Qiu, F. (2018). Characterization of the *in vivo* and *in vitro* metabolites of linarin in rat biosamples and intestinal flora using ultra-high performance liquid chromatography coupled with quadrupole time-of-flight tandem mass spectrometry. *Molecules*, 23(9), 2140.
- Guo, C. X., Zhang, H., Guan, X., & Zhou, Z. Q. (2019). The anti-aging potential of neohesperidin and its synergistic effects with other citrus flavonoids in extending chronological lifespan of *Saccharomyces cerevisiae* BY4742. *Molecules (Basel, Switzerland)*, 24(22), 4093.
- Indulkar, A. S., Lou, X. C., Zhang, G., & Taylor, L. S. (2019). Insights into the dissolution mechanism of ritonavir-copovidone amorphous solid dispersions: Importance of congruent release for enhanced performance. *Molecular Pharmaceutics*, 16(3), 1327–1339.
- Li, P. W., Luo, S., Xiao, L. Y., Tian, B. L., Wang, L., Zhang, Z. R., & Zeng, Y. C. (2019). A novel gemcitabine derivative-loaded liposome with great pancreas-targeting ability. *Acta Pharmacologica Sinica*, 40(11), 1448–1456.
- Li, X. J., Lin, Y. H., Zhou, H. Y., Li, Y., Wang, A. M., Wang, H. X., & Zhou, M. S. (2017). Puerarin protects against endothelial dysfunction and end-organ damage in Ang II-induced hypertension. *Clinical and Experimental Hypertension (New York, N.Y. : 1993)*, 39(1), 58–64.
- Li, Y., Guang, C. X., Zhao, N., Feng, X. C., & Qiu, F. (2019). LC-MS/MS method for simultaneous determination of linarin and its metabolites in rat plasma and

- liver tissue samples: Application to pharmacokinetic and liver tissue distribution study after oral administration of linarin. *Molecules (Basel, Switzerland)*, 24(18), 3342.
- Mesallati, H., Umerska, A., Paluch, K. J., & Tajber, L. (2017). Amorphous polymeric drug salts as ionic solid dispersion forms of ciprofloxacin. *Molecular Pharmaceutics*, 14(7), 2209–2223.
- Onoue, S., Sato, H., Ogawa, K., Kawabata, Y., Mizumoto, T., Yuminoki, K., Hashimoto, N., & Yamada, S. (2010). Improved dissolution and pharmacokinetic behavior of cyclosporine A using high-energy amorphous solid dispersion approach. *International Journal of Pharmaceutics*, 399(1–2), 94–101.
- Sheng, Q. Q., Fang, X. Y., Zhao, H. J., Zhu, Z. L., & Zhao, L. G. (2018). Seasonal changes in the major flavonoids and anti-tumor capacity of the methanol extracts of carpinus. *Current Topics in Nutraceutical Research*, 16(3), 179–187.
- Rumondor, A. C., Marsac, P. J., Stanford, L. A., & Taylor, L. S. (2009). Phase behavior of poly (vinylpyrrolidone) containing amorphous solid dispersions in the presence of moisture. *Molecular Pharmaceutics*, 6(5), 1492–1505.
- Shao, S. Y., Ting, Y., Wang, J., Sun, J., & Guo, X. F. (2020). Characterization and identification of the major flavonoids in *Phyllostachys edulis* leaf extract by UPLC–QTOF–MS/MS. *Acta Chromatographica*, 32(4), 1–10.
- Sun, X. X., & Jin, N. (2009). Research progress on liposomes. *Journal of Medical Research*, 38(12).
- Tai, K. D., Rappolt, M., He, X. Y., Wei, Y., Zhu, S. X., Zhang, J. B., ... Yuan, F. (2019). Effect of β -sitosterol on the curcumin-loaded liposomes: Vesicle characteristics, physicochemical stability, *in vitro* release and bioavailability. *Food Chemistry*, 293, 92–102.
- Tang, W. Z., Wang, Y. A., Gao, T. Y., Wang, X. J., & Zhao, Y. X. (2017). Identification of C-geranylated flavonoids from *Paulownia catalpifolia* Gong Tong fruits by HPLC–DAD–ESI–MS/MS and their anti-aging effects on 2BS cells induced by H₂O₂. *Chinese Journal of Natural Medicines*, 15(5), 384–391.
- Tian, J. Y., Guo, F. J., Chen, Y. Y., Li, Y. Q., Yu, B. B., & Li, Y. (2019). Nanoliposomal formulation encapsulating celecoxib and genistein inhibiting COX-2 pathway and Glut-1 receptors to prevent prostate cancer cell proliferation. *Cancer Letters*, 448, 1–10.
- Uifălean, A., Schneider, S., Gierok, P., Ionescu, C., Iuga, C. A., & Lalk, M. (2016). The impact of soy isoflavones on mcf-7 and mda-mb-231 breast cancer cells using a global metabolomic approach. *International Journal of Molecular Sciences*, 17(9), 1443.
- Vasconcelos, T., Sarmiento, B., & Costa, P. (2007). Solid dispersions as strategy to improve oral bioavailability of poor water soluble drugs. *Drug Discovery Today*, 12(23–24), 1068–1075.
- Vergara, D., & Shene, C. (2019). Encapsulation of lactoferrin into rapeseed phospholipids based liposomes: Optimization and physicochemical characterization. *Journal of Food Engineering*, 262(DEC.), 29–38.
- Wang, C. L., Li, Y., Chen, H. L., Zhang, J., Zhang, J., Qin, T., ... Yang, J. (2017). Inhibition of CYP4A by a novel flavonoid FLA-16 prolongs survival and normalizes tumor vasculature in glioma. *Cancer Letters*, 402, 131–141.
- Wang, J. S., Fu, B., Lu, F. C., Hu, X. W., Tang, J. S., & Huang, L. X. (2018). Inhibitory activity of linarin on osteoclastogenesis through receptor activator of nuclear factor κ B ligand-induced NF- κ B pathway. *Biochemical and Biophysical Research Communications*, 495(3), 2133–2138.
- Wang, J., Xun, J., Zhang, T. J., & Amp, N. (2013). Preparation of linarin solid dispersion and its properties. *Drugs & Clinic*, 28(06), 870–873.
- Xie, G. Y., Yang, J., Wei, X. N., Xu, Q. H., & Qin, M. J. (2020). Separation of acteoside and linarin from *Buddlejae Flos* by high-speed counter current chromatography and their anti-inflammatory activities. *Journal of Separation Science*, 43(8), 1450–1457.
- Yi, Y. S. (2018). Regulatory roles of flavonoids on inflammasome activation during inflammatory responses. *Molecular Nutrition & Food Research*, 62(13), e1800147.
- Zanoaga, O., Braicu, C., Jurj, A., Rusu, A., Buiga, R., & Berindan-Neagoe, I. (2019). Progress in research on the role of flavonoids in lung cancer. *International Journal of Molecular Sciences*, 20(17), 4291.
- Zeng, Y. C., Li, S., Liu, C., Gong, T., Sun, X., Fu, Y., & Zhang, Z. R. (2017). *Soluplus micelles* for improving the oral bioavailability of scopoletin and their hypouricemic effect *in vivo*. *Acta Pharmacologica Sinica*, 38(3), 424–433.
- Zhen, Z. G., Ren, S. H., Ji, H. M., Ma, J. H., Ding, X. M., Feng, F. Q., ... Jia, L. (2017). Linarin suppresses glioma through inhibition of NF- κ B/p65 and up-regulating p53 expression *in vitro* and *in vivo*. *Biomedicine & Pharmacotherap*, 95, 363–374.